Comparison of Impulsive and Compliant Contact Models for Impact Analysis in Biomechanical Multibody Systems

Josep M. Font-Llagunes[*], József Kövecses[†], Rosa Pàmies-Vilà[*], Ana Barjau[*]

[*] Department of Mechanical Engineering
Universitat Politècnica de Catalunya
Diagonal 647, 08028 Barcelona, Spain
e-mail: josep.m.font@upc.edu,
rosa.pamies@upc.edu, ana.barjau@upc.edu

[†] Department of Mechanical Engineering
Centre for Intelligent Machines, McGill University
817 Sherbrooke St. West
H3A 2K6 Montréal, Canada
e-mail: jozsef.kovecses@mcgill.ca

ABSTRACT

Two approaches are used when studying impact problems: impulsive ones and compliant ones. In an impulsive approach, the time interval where the collision takes place is considered to be negligible, and so the system configuration is assumed to be constant. The final mechanical state of the colliding system is obtained directly from the initial one through algebraic equations and energy dissipation assumptions. In a compliant approach, the colliding surfaces are modelled through springs and dampers (usually nonlinear), and the equations of motion are integrated during the impact time interval to obtain the final state. Though both approaches have been widely used in the field of biomechanics, no comparative study can be found in the literature that could justify choosing one or another. In this paper, we present both approaches and compare them when applied to two examples related to gait problems: a passive walker and a simple model of crutch locomotion. We will show that the results are really close whenever nonsliding conditions are assumed at the impact points.

Keywords: Biomechanics, human locomotion, contact dynamics, impact.

1 INTRODUCTION

The analysis of the impact dynamics is a major subject in biomechanics, since this phenomenon is often present when the human body interacts with the environment. This is the case, for example, of the heel strike in human walking that occurs at the end of the swing phase. When heel strike occurs, there is a sudden change of the velocities of the body and new constraint conditions are imposed on the system [4,13].

There are two main approaches for the dynamics analysis of impact in the literature: *impulsive* and *compliant* [19]. The use of one or the other depends on the purpose of the study. Surprisingly, no comparison between both approaches when applied to biomechanics can be found in the existing literature. The aim of this paper is to compare the performance of impulsive and compliant contact formulations using two different examples of impacts in biomechanical systems.

Impulsive approaches assume that the contact interaction is instantaneous –compared to the time scale of the continuous finite motion of the system– and, therefore, the system configuration is constant during the impact interval. In this case, the integrated version of the equations of motion –that is, the impulse-momentum equations– are used to solve the forward dynamics of the multibody system. This formulation provides a reasonable and easy-to-implement representation of the impact phenomenon. The solution to the forward dynamics is achieved simply by solving a set of algebraic equations and, therefore, it is very helpful to obtain performance indicators of the impact such as the mechanical energy loss or the magnitude of contact impulses [4]. When applying this methodology, only pre- and post-impact information is used in principle. Impulsive formulations have been widely used for the analysis of passive dynamic walking [3,16], and also to understand the physical principles of human locomotion [12,13].

In compliant approaches, the dynamics of contact interaction is solved continuously in time. Therefore, the configuration is allowed to change during the impact interaction. When contact is detected –usually from geometric information–, the contact forces are added to the differential equations of motion. This analysis requires a model giving the variation of the compliant contact forces during the impact interval as a function of the system state [6,10]. An advantage of using compliant descriptions of contact forces is that their evolution is followed during the impact interval, and thus, an estimation of the maximum force occurring during the impact can be obtained. This is important in biomechanics because contact forces are transmitted to joints and are responsible for fatigue and joint damage. Compared to impulsive models, however, the use of compliant formulations results in a computationally costly way to solve the forward dynamics, since it requires the integration of the system equations of motion. Moreover, a very small time step is needed due to the rapid variation of forces and velocities within the impact interval. Another drawback is that such models require a characterization of the geometry and the material properties of the bodies in contact in order to obtain stiffness and damping parameters.

In this work, we compare the use of both approaches to analyze situations where constraints are suddenly imposed on the biomechanical system. The two application examples are the heel-strike impact of a passive dynamic compass-walker and the impact of the crutch tip with the ground at the end of the foot-stance phase of crutch locomotion. For the sake of simplicity, nonsliding conditions at the contact point will be assumed in all cases. The energy loss at impact, the contact impulses and the post-impact velocities will be used as indicators to compare the performance of both contact formulations using the same pre-impact states. We will analyze how impact configuration and dynamic parameters of the model influence the performance of the two contact models.

2 DYNAMICS MODELLING OF BIOMECHANICAL MULTIBODY SYSTEMS

The dynamics of the compass walker (Figure 1a) and the subject walking with crutches (Figure 1b) are modelled using independent coordinates. Vector $\mathbf{q}$ is the $(n\times 1)$ array representing the configuration of the system, and $\dot{\mathbf{q}}$ is the $(n\times 1)$ array of generalized velocities. According to Figure 1, n=4 for the compass walker, and n=6 for the crutch walker model.

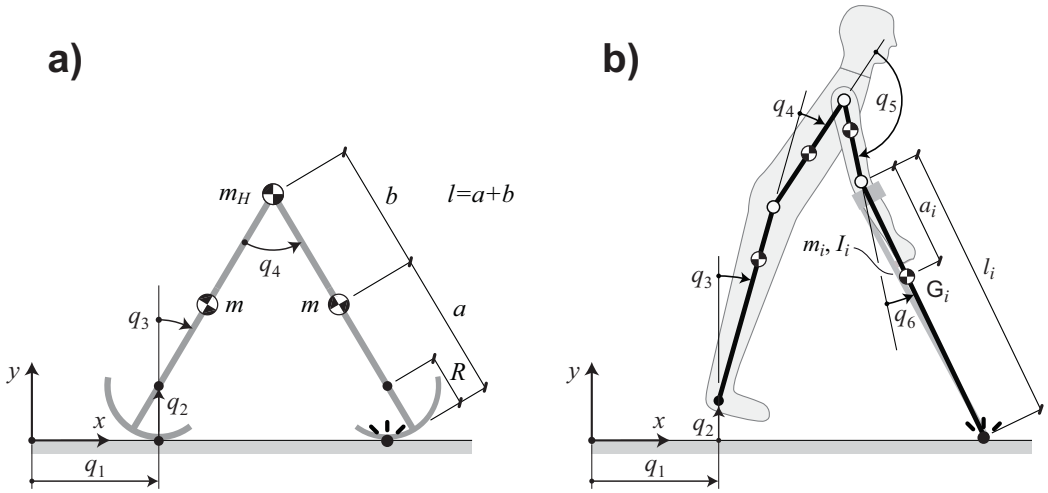

Figure 1. Application examples: (a) Compass-gait biped with circular feet. (b) Planar model of a subject walking with crutches.

Both systems are assumed to have two-dimensional motion on the sagittal plane. Using a Lagrangian formalism, the general n equations of motion of such systems can be expressed as:

$$\mathbf{M}(\mathbf{q})\ddot{\mathbf{q}}+\mathbf{c}(\mathbf{q},\dot{\mathbf{q}})=\mathbf{f}_A+\mathbf{f}_C\,, \tag{1}$$

where $\mathbf{M}$ is the mass or inertia matrix, $\mathbf{c}$ represents the Coriolis and centrifugal effects, and $\mathbf{f}_A$ and $\mathbf{f}_C$ stand for the generalized applied and constraint –contact– forces, respectively. In what follows, the formulations for both impulsive and compliant contact modelling are outlined.

3 IMPULSIVE FORMULATION

Impulsive approaches consider the impact interval to be very short in the characteristic time scale of the finite motion of the system. Therefore, the configuration $\mathbf{q}$ is assumed to be constant during the "instantaneous" interaction, whereas velocities experience finite changes and accelerations reach infinite values. This latter fact is the reason for dealing with contact force impulses rather than with contact forces, and for using *in principle* the integrated form of the equations of motion, which are algebraic equations.

The main drawback in an impulsive approach is the collision end detection [2]. Neither the final state nor the final values of the impulses are in general known beforehand, and an "end-collision criterion" has to be defined. The most common formulation of the collision end is done through restitution coefficients (kinematic, kinetic or energetic) [17,19] taking values in the interval (0, 1). Among them, the first two may be in general energetically inconsistent whenever friction is not neglected [1], and have to be used cautiously.

The impact problem studied in this paper is that of a single-point impact with the ground in bipedal or crutch locomotion. Under the assumption of nonsliding conditions, the collision end criterion is that of final zero velocity for the impact point (called point Q from now on), since new constraints are established on the foot or the crutch after impact.

Considering that impact takes place in the $[\,t^-, t^+\,]$ interval –where t^- and t^+ stand for the so-called pre- and post-impact instants, respectively– and that the system has n degrees of freedom (DOF) $\dot{\mathbf{q}}$, the velocity of the colliding point $\mathbf{v}(Q)$ can be related to the generalized velocities through the $(3\times n)$ Jacobian matrix as $\mathbf{v}(Q) = \mathbf{A}(\mathbf{q})\dot{\mathbf{q}}$. At impact configuration, matrix $\mathbf{A}$ can be decomposed into a $(1\times n)$ vector and a $(2\times n)$ matrix specific for the normal and tangential components of $\mathbf{v}(Q)$:

$$\mathbf{v}(Q) = \begin{Bmatrix} v_n(Q) \\ \mathbf{v}_t(Q) \end{Bmatrix} = \begin{bmatrix} \mathbf{A}_n \\ \mathbf{A}_t \end{bmatrix} \dot{\mathbf{q}}, \tag{2}$$

and the collision end condition can be written as:

$$\mathbf{v}^+(Q) = \mathbf{A}\dot{\mathbf{q}}^+ = \mathbf{0}, \tag{3}$$

which represents the constraint condition of the system at post-impact time t^+, i.e., the fact that the colliding point stays in contact with the ground without slipping after impact. The impulsive approach used in this work starts with the general equations of motion as in Equation (1). In our case, we assume that the only impulsive forces are the ground contact forces (normal and tangential forces) at point *Q*. The Coriolis and centrifugal effects and the other forces are essentially non-impulsive. Thus, Equation (1) can be rewritten as:

$$\mathbf{M}\, d\dot{\mathbf{q}} = \mathbf{A}_n^T\, dP_n + \mathbf{A}_t^T\, d\mathbf{P}_t = \mathbf{A}^T \begin{Bmatrix} dP_n \\ d\mathbf{P}_t \end{Bmatrix}, \tag{4}$$

where dP_n and $d\mathbf{P}_t$ are the differential normal and tangential contact impulses at *Q*. The total impulses P_n and $\mathbf{P}_t$ can be obtained as

$$P_n = \int_-^+ dP_n = \int_-^+ F_n(Q)\,dt \;\;,\;\; \mathbf{P}_t = \int_-^+ d\mathbf{P}_t = \int_-^+ \mathbf{F}_t(Q)\,dt, \tag{5}$$

where F_n and $\mathbf{F}_t$ are the normal and tangential contact forces at *Q*, respectively.

3.1 All-algebraic Method

As mentioned before, what is usually called "impulsive formulation" relies on algebraic equations obtained from Equation (4) through a time integration over the impact:

$$\mathbf{M}\,\Delta\dot{\mathbf{q}} = \mathbf{A}^T \begin{Bmatrix} P_n \\ \mathbf{P}_t \end{Bmatrix} \Rightarrow \dot{\mathbf{q}}^+ = \dot{\mathbf{q}}^- + \mathbf{M}^{-1}\mathbf{A}^T \begin{Bmatrix} P_n \\ \mathbf{P}_t \end{Bmatrix}, \tag{6}$$

where the superscripts "–" and "+" indicate at pre- and post-impact time, respectively. Using Equation (1), the impulses can be obtained as:

$$\begin{Bmatrix} P_n \\ \mathbf{P}_t \end{Bmatrix} = -\left(\mathbf{A}\mathbf{M}^{-1}\mathbf{A}^T\right)^{-1} \mathbf{A}\,\dot{\mathbf{q}}^- . \tag{7}$$

The final velocities are obtained by substituting back these final impulses into Equation (6):

$$\dot{\mathbf{q}}^+ = \left[\mathbf{I} - \mathbf{M}^{-1}\mathbf{A}^T\left(\mathbf{A}\mathbf{M}^{-1}\mathbf{A}^T\right)^{-1}\mathbf{A}\right]\dot{\mathbf{q}}^- . \tag{8}$$

The last equation can be expressed through the "Space of Admissible/Constrained Motion" projectors, $\mathbf{P}_a$ and $\mathbf{P}_c$ respectively [4,11], as

$$\dot{\mathbf{q}}^+ = \left(\mathbf{I} - \mathbf{P}_c\right)\dot{\mathbf{q}}^- \equiv \mathbf{P}_a\,\dot{\mathbf{q}}^- . \tag{9}$$

3.2 Integrative Method

The all-analytical solution presented in Section 3.1 does not give any insight about the time history of the normal and tangential forces at *Q*, their associated work W_n and W_t, and that of $\mathbf{v}(Q)$ during the impact, as time is not actually a variable in that kind of model. However, Equation (4) suggests another variable that could be used to trace the $\mathbf{v}(Q)$ evolution.

As the tangential velocity of the colliding point is taken to be zero throughout the whole collision, $\mathbf{A}_t d\dot{\mathbf{q}} = \mathbf{0}$, the tangential differential impulse is proportional to the normal one. From Equation (4):

$$d\mathbf{P}_t = -\left(\mathbf{A}_t\mathbf{M}^{-1}\mathbf{A}_t^T\right)^{-1}\mathbf{A}_t\mathbf{M}^{-1}\mathbf{A}_n^T\,dP_n , \tag{10}$$

and so the right hand side of Equation (4) is strictly proportional to dP_n:

$$\mathbf{M}\,d\dot{\mathbf{q}} = \left[\mathbf{I} - \mathbf{A}_t^T\left(\mathbf{A}_t\mathbf{M}^{-1}\mathbf{A}_t^T\right)^{-1}\mathbf{A}_t\mathbf{M}^{-1}\right]\mathbf{A}_n^T\,dP_n . \tag{11}$$

Thus, the normal impulse at *Q* appears as a "natural variable" of integration. We can then proceed to a numerical integration of Equation (10). Though the final value of P_n is not known beforehand, the end of the integration is defined through the condition $\mathbf{v}^+(Q) = \mathbf{0}$.

The evolution of W_n and $\mathbf{v}(Q)$ as a function of P_n can provide another interesting tool to compare impulsive with compliant approaches, though not as straightforward as those of energy loss at impact and post-impact velocities.

$$W_n = \int_0^{P_n} v_n(Q)\,dP_n . \tag{12}$$

4 COMPLIANT FORMULATION

Compliant formulations, or *penalty* formulations, consider the impact phase with finite duration. These techniques relax the contact constraints and replace them with force models that establish an explicit representation of the contact forces (both normal and tangential). The associated generalized forces appear on the right hand side of Equation (1). The use of those formulations is helpful to obtain a realistic-looking motion behaviour. Nevertheless, the required model parameters are not always easy to identify and, moreover, their physical meaning could be sometimes questionable.

4.1 Normal Contact Force Model

The simplest compliant formulations for the normal force are the Maxwell and the Kelvin-Voigt models [7,19], where the contact force is represented through a series or parallel linear spring-damper element, respectively. They have been widely used due to their simplicity. However, they do not express the nonlinear relationship between force and indentation when contact occurs [15].

In this work, we use a nonlinear Hunt-Crossley model to account for that relationship [8,15]. For the case of single-point contact of spherical surfaces, the normal contact force F_n has the following expression:

$$F_n = k_n \left|\delta_n\right|^{3/2} + \chi \left|\delta_n\right|^{3/2} \dot{\delta}_n \quad , \tag{13}$$

where k_n is the generalized normal stiffness according to Hertz theory [9] –and it depends on the materials properties and the surfaces curvature–, δ_n (>0) and $\dot{\delta}_n$ are the normal indentation between bodies and its time derivative, and χ is the hysteresis damping factor. In this paper, the contacts are modelled as sphere-to-plane. Thus, the generalized stiffness k_n can be calculated as [9,19]

$$k_n = \frac{4E^* \sqrt{R_{sph}}}{3} \quad , \tag{14}$$

where R_{sph} is the radius of the sphere and E^* is the effective Young's modulus, which can in turn be calculated through:

$$E^* = \left[\frac{1-\nu_{sph}^2}{E_{sph}} + \frac{1-\nu_{pl}^2}{E_{pl}} \right]^{-1} \quad . \tag{15}$$

E_{sph} and E_{pl} stand for the Young's modulus of the sphere and plane materials, and ν_{sph} and ν_{pl} stand for the Poisson's ratio of the same materials. The damping parameter can be obtained as a function of the restitution coefficient *e* and the pre-impact normal velocity $\dot{\delta}_n^-$ as [15]

$$\chi = \frac{3k_n \left(1-e^2\right)}{4\dot{\delta}_n^-} \quad . \tag{16}$$

4.2 Tangential Contact Force Model

The tangential contact force $\mathbf{F}_t$ is described through a Coulomb's dry friction model accounting also for the compliance of materials in the tangential direction. Assuming nonsliding conditions in the contact area, this force is

$$\mathbf{F}_t = -k_t \left|\delta_n\right|^{1/2} \boldsymbol{\delta}_t \quad , \tag{17}$$

where k_t is the tangential stiffness according to Hertz theory [5,9], and $\boldsymbol{\delta}_t$ the tangential displacement. The stiffness parameter k_t can be calculated as [5,9]

$$k_t = 8G^* \sqrt{R_{sph}} \quad , \tag{18}$$

where G^* is the effective rigidity modulus of materials, which can in turn be calculated through:

$$G^* = \left[\frac{2-\nu_{sph}}{G_{sph}} + \frac{2-\nu_{pl}}{G_{pl}} \right]^{-1} \quad . \tag{19}$$

G_{sph} and G_{pl} stand for the rigidity modulus of the sphere and plane materials. Note that Equation (16) is only valid if $\left|\mathbf{F}_t\right| \le \mu_s F_n$, where μ_s is the static coefficient of friction. When that condition is broken or a relative tangential velocity between the bodies in contact appears, the $\mathbf{F}_t$ force is formulated according to Coulomb's model as $\mathbf{F}_t = -\mu_d F_n \left(\mathbf{v}_t / \left|\mathbf{v}_t\right|\right)$, where μ_d is the dynamic coefficient of friction.

5 APPLICATION EXAMPLES AND RESULTS

In this section, the two aforementioned models are used to simulate the dynamics of the impact of the two examples shown in Figure 1. The results obtained applying one or the other formulation will be compared to asses the similarity regarding the impact dynamics.

5.1 Compass-gait Biped

The compass walker presented in Figure 1a is composed of two straight legs of length l = 1 m and mass m = 5 kg. The centre of mass of each leg is at a distance b = 0.5 m from the hip. The radius of the feet is R (this parameter will be varied in simulations) and the hip is modelled as a point mass m_H = 10 kg located at the revolute joint between the two legs. In this model, coordinates q_1 and q_2 indicate the position of the centre of the stance foot, coordinate q_3 denotes the absolute orientation of the stance leg, and q_4 is the relative angle between the two legs. The pre-impact state $\left(\mathbf{q}^-, \dot{\mathbf{q}}^-\right)$ is defined as follows:

- Pre-impact configuration: $\mathbf{q}^- = \begin{bmatrix} 0 & 0 & q_3 & q_4 = 2q_3 \end{bmatrix}^T$, where q_3 will be varied in the analysis.
- Stance foot rolling on the ground without slipping, that is, $\dot{q}_1^- = R\dot{q}_3^-$ and $\dot{q}_2^- = 0$, with $\dot{q}_3^- = 1$ rad/s .
- Colliding point not slipping at pre-impact time, which implies that $\dot{q}_4^- = 0$.

To evaluate the behaviour of both impact formulations for different pre-impact configurations, the q_3 coordinate is varied within the interval $\left[0^o, 30^o\right]$. Note that this is equivalent to simulating different step lengths. In this case, the radius of the feet is kept constant, R = 0.25 m. The results are shown in Figure 2.

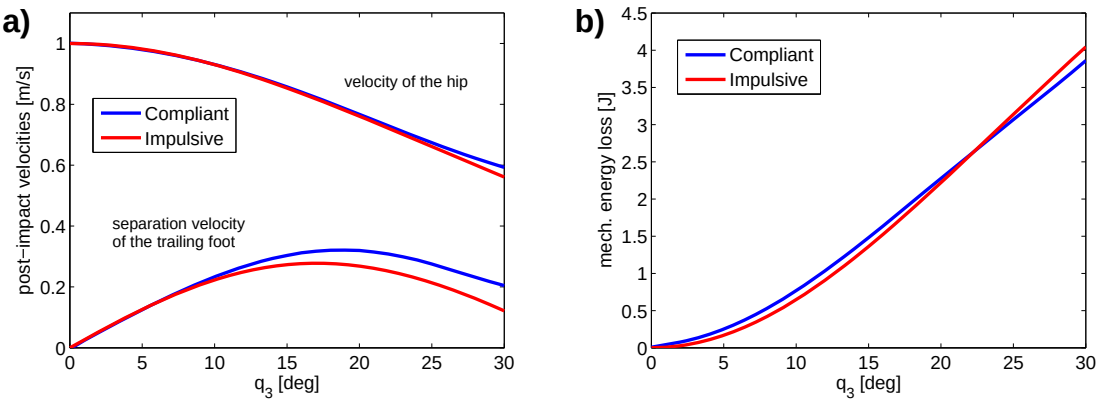

Figure 2. (a) Post-impact separation velocity of the trailing foot and post-impact velocity of the hip as a function of q_3 using both approaches. (b) Mechanical energy loss at impact as a function of q_3 using both approaches.

Figure 2a shows the post-impact separation velocity of the trailing (or rear) foot, i.e., $\dot{q}_2^+$, and the post-impact velocity of the hip point using both approaches. Both contact models yield similar results. The curves showing the post-impact velocity of the hip almost overlap. The vertical velocity of the rear foot also presents similar values for $q_3 \in \left[0^o, 10^o\right]$, but there is some discrepancy in the rest of the interval. Nevertheless, the tendency of both curves for increasing values of q_3 is comparable. From the results above, it can also be concluded that the separation velocity reaches its maximum value for an angle q_3 between 15º to 20º.

Figure 2b shows the mechanical energy loss at impact using both contact models. In the compliant approach, this energy loss equals the work of the contact forces. As for the impulsive approach, this energy loss is calculated as the change of kinetic energy since the configuration, and therefore the potential energy, are assumed constant. From these results, the main conclusion is that both methods estimate a very similar amount of energy loss for each impact configuration $\mathbf{q}^-$. This was an expected but not obvious result if we take into account the nature of both models. In the impulsive approach, the change of energy is due to the sudden imposition of the constraint expressed in Equation (3), whereas in

the compliant approach all constraints are relaxed and contact forces are modelled taking into account the material properties and geometry of the bodies in contact, Equations (13) and (17). From the plot in Figure 2b, it can be clearly concluded that the energy loss at impact for a compass walker increases with angle q_3 and, therefore, with the step length [4,12]. Note that there is a clear correlation between the energy loss and the decrement of the velocity of the hip (which is equal to 1 m/s before impact for all cases).

The performance of both approaches to a change in a geometric parameter of the system has also been evaluated. We have restricted our study to the radius, which has been varied from 0.05 to 1 m (leg length). The pre-impact configuration is $q_3 = 20^o$ and $q_4 = 2q_3 = 40^o$. The Jacobian matrix **A** of the constraints imposed in the impulsive formulation depends on that parameter, and also the stiffness parameters k_n and k_t of the compliant contact forces. The results are shown in Figure 3.

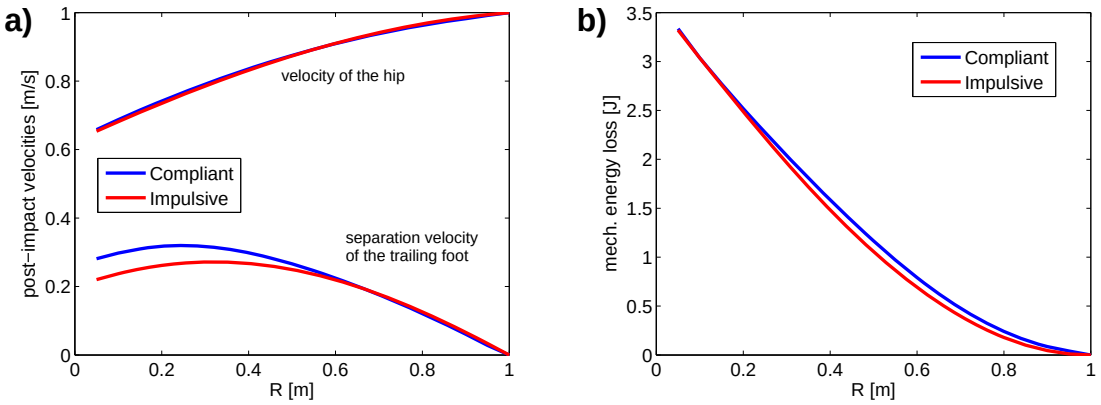

Figure 3. (a) Post-impact separation velocity of the trailing foot and post-impact velocity of the hip as a function of R using both approaches. (b) Mechanical energy loss at impact as a function of R using both approaches.

Figure 3a shows the same aforementioned post-impact velocities as a function of *R*. Again, the two curves for the post-impact velocity of the hip almost overlap. As for the separation velocity of the trailing foot, the curves overlap for $R > 0.5$ m, whereas for lower radii there is a slight difference.

Figure 3b shows the energy loss at impact using the two contact models as a function of *R*. The results are again very close. Note that in general, the compliant approach estimates more energy loss rather than the impulsive one. The reason could be that a contact force model is also included on the rear foot in the compliant approach, whereas in the impulsive case this contact is relaxed. From Figure 3b, it can be concluded that the radius of the foot is a key parameter to reduce energy losses at heel strike. Large radii lead to lower energy losses, and when $R = l = 1$ m no energy is lost because there is no impact at all. This results are in clear agreement with the works [14,16].

5.2 Crutch Locomotion

The planar model of the subject with the crutches, Figure 1b, is composed of four segments (legs , torso, upper arms, and arms plus crutches) linked by revolute joints, modelling the hip, shoulder and elbow joints. Coordinates q_1 and q_2 indicate the position of the feet, coordinate q_3 denotes the absolute orientation of the legs, q_4 is the relative angle between torso and legs, q_5 is the relative angle between upper arms and torso, and q_6 is the relative angle between crutches and upper arms. The anthropometric parameters are the ones for a subject whose total mass is 70 kg and the height is 1.75 m according to [20]. The crutches have a mass of 1.2 kg and are 1 m long. These parameters are summarized in Table 1.

	Legs	Torso	Upper Arms	Arms+crutches
m (kg)	22.54	40.46	3.92	4.28
I_G (kg·m^2)	2.07	2.66	0.044	0.433
l (m)	0.93	0.51	0.33	1.25
a (m)	0.51	0.34	0.14	0.33

Table 1. Anthropometric parameters of the model of a subject with crutches.

The pre-impact state $\left(\mathbf{q}^-, \dot{\mathbf{q}}^-\right)$ is defined according to kinematic studies of subjects walking with crutches [18]. As for configuration $\mathbf{q}^-$, the rear foot will be at position $\left(q_1 = 0,\, q_2 = 0\right)$, q_5 will be equal to 150º in all cases, and q_6 will be that needed to guarantee the crutch-ground contact; the other two coordinates will be varied within reasonable intervals. Concerning pre-impact velocities, kinematic studies show that relative angular velocities associated with the hip, shoulder and elbow joints are approximately zero before crutch tip impact [18]. Thus, the only non-zero generalized velocity is $\dot{q}_3^-$, and this can take different values depending on the subject specific pathology. For the sake of simplicity, we have taken a value of 1 rad/s.

The behaviour of both impact formulations for different pre-impact leg angles q_3 within the interval $\left[5^o,\, 30^o\right]$ has been explored. The hip angle has been kept constant and equal to $q_4 = +10^o$. The results are shown in Figure 4.

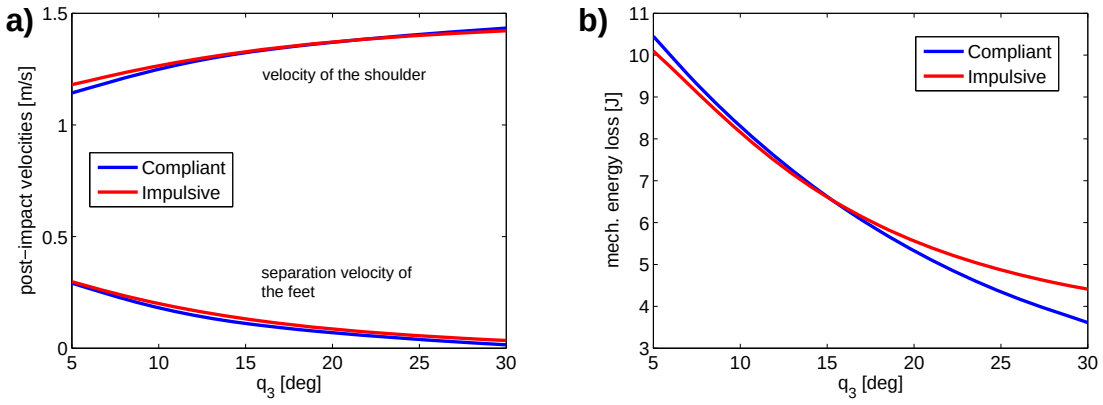

Figure 4. (a) Post-impact separation velocity of the feet and post-impact velocity of the shoulder as a function of q_3 using both approaches. (b) Mechanical energy loss at impact as a function of q_3 using both approaches.

Figure 4a shows the post-impact velocity of the shoulder joint and the vertical velocity of the feet as a function of the legs angle q_3. Both curves almost overlap, which means that the post-impact kinematics are very close in the two contact approaches. Moreover, the separation velocity decreases when angle q_3 increases. Therefore, a lower angle facilitates lifting the feet up, thus decreasing the push-off effort in swing-through crutch gait. However, for low values of q_3, the post-impact velocity of the shoulder is lower.

Figure 4b shows the loss of mechanical energy. The two curves show a similar tendency. For angles $q_3 \in \left[5^o, 15^o\right]$ the two contact approaches lead to very close results in terms of energetic losses. For higher angles the two curves differ a little bit, although the tendency remains the same. From the results obtained, one can conclude that a higher angle q_3 leads to less energy losses at impacts when walking with crutches. Note that in general less energy loss leads to a higher velocity of the shoulder after impact.

The behaviour of both impact formulations for different hip relative angles q_4 within the interval $\left[-10^o,\, 20^o\right]$ has also been studied. The absolute angle of the legs has been kept constant and equal to $q_3 = +10^o$. The results are shown in Figure 5.

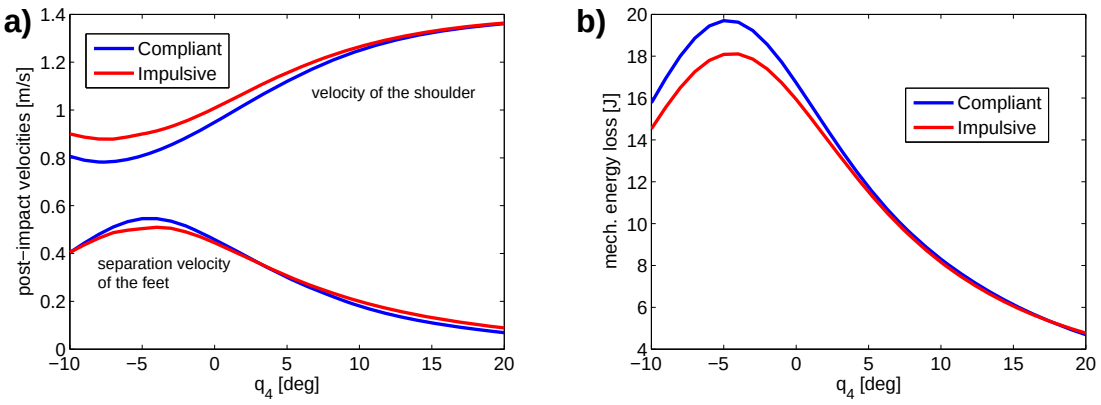

Figure 5. (a) Post-impact separation velocity of the feet and post-impact velocity of the shoulder as a function of q_4 using both approaches. (b) Mechanical energy loss at impact as a function of q_4 using both approaches.

Figure 5a shows the post-impact velocity of the shoulder joint and the vertical velocity of the feet as a function of the hip angle q_4. Again, both contact formulations lead to similar values of the post-impact kinematics. The separation velocity of the feet is maximum when the torso leans slightly backwards with respect to the legs, that is, for $q_4 \approx -5^o$. Conversely, the velocity of the shoulder after impact increases when the torso leans forward.

Figure 5b shows the loss of mechanical energy of the biomechanical model using the both approaches. Both curves show the same tendency, and they overlap for hip angles $q_4 \geq 0$. For negative angles –that is, when the torso leans backwards with respect to the legs– the models estimate slightly different energetic losses. Note that in Figure 4b energy losses are estimated to be higher when the impulsive approach is used, whereas in Figure 5b it is the contrary. It is important to remark that in this case, the velocity of the shoulder after the impact is also related to the energetic loss –note the coincident tendency of the curves–: higher energetic losses correspond to lower velocities of that joint.

6 CONCLUSIONS

In this work, we have presented two different approaches for the forward dynamics analysis of impacts in multibody biomechanical systems. In the first one, the impact condition is established through impulsive bilateral constraints, and equations of motion integrated over the impact interval are used. In the second approach, compliant contact models are used to define an explicit relationship between the normal and tangential forces and the system state. These models depend on the materials properties and geometry of the bodies in contact.

We have compared the performance of both approaches in two impact situations in biomechanical systems: the heel strike impact of a compass-gait walker and the impact of the crutch tip in swing-through gait. We have used post-impact velocities of the system and the mechanical energy loss at impact as indicators to compare the results of the dynamic forward simulation. We have varied dynamic parameters and configuration in order to see their effect in the performance of both approaches. The main conclusion is that the results are surprisingly similar taking into account the different nature of the contact approaches. Therefore, choosing one or the other will not affect significantly the result of the analysis. The main advantage of the impulsive formulations is their simplicity, since forward dynamics can be solved algebraically. However, no information on the real contact forces can be obtained. Compliant formulations are computationally costly, but the evolution of the contact forces during the impact interval can be obtained.

REFERENCES

[1] AGULLÓ BATLLE, J., AND BARJAU CONDOMINES, A. Rough collisions in multibody systems. *Mech. Mach. Theory 26*, 6 (1991), 656-677.

[2] BATLLE, J. A. Termination conditions for three-dimensional inelastic collisions in multibody systems. *Int. J. of Impact Eng. 25*, (2001), 615-629.

[3] COLLINS, S. H., WISSE, M., AND RUINA, A. A three-dimensional passive dynamic walking robot with two legs and knees. *International Journal of Robotics Research 20*, 7 (2001), 607–615.

[4] FONT-LLAGUNES, J. M., AND KÖVECSES, J. Dynamics and energetics of a class of bipedal walking systems. *Mechanism and Machine Theory 44*, 11 (2009), 1999-2019.

[5] GARCÍA-REYERO VIÑAS, J. M. *Rough Collisions with Finite Tangential Stiffness*, PhD Thesis. Barcelona: Technical University of Catalonia (UPC), 2000.

[6] GILCHRIST, L. A., AND WINTER, D.A. A two-part, viscoelastic foot model for use in gait simulations. *Journal of Biomechanics 29*, 6 (1996), 795-798.

[7] GOLDSMITH, W. *Impact: The Theory and Physical Behaviour of Colliding Solids*. London: Edward Arnold Publishers Ltd., 1960.

[8] HUNT, K. H., AND CROSSLEY, F. R. E. Coefficient of restitution interpreted as damping in vibroimpact. *Journal of Applied Mechanics 42*, 2 (1975), 440-445.

[9] JOHNSON, K. L. *Contact Mechanics*, 6th ed. Cambridge: Cambridge University Press, 1996.

[10] KAPLAN, M. L., AND HEEGAARD, J. H. Energy-conserving impact algorithm for the heel-strike phase of gait. *Journal of Biomechanics 33*, 6 (2000), 771-775.

[11] KÖVECSES, J. Dynamics of Mechanical Systems and the Generalized Free-Body Diagram—Part I: General Formulation. *Journal of Applied Mechanics 75*, 6 (2008), 061012, 1-12.

[12] KUO, A. D. Energetics of actively powered locomotion using the simplest walking model. *Journal of Biomechanical Engineering 124*, 1 (2002), 113-120.

[13] KUO, A. D., DONELAN, J. M., AND RUINA, A. Energetic consequences of walking like an inverted pendulum: Step-to-step transitions. *Exercise and Sport Sciences Review 33*, 2 (2005), 88-97.

[14] KWAN, M., AND HUBBARD, M. Optimal foot shape for a passive dynamic biped. *Journal of Theoretical Biology 248*, 2 (2007), 331-339.

[15] LANKARANI, H. M., AND NIKRAVESH, P. E. Continuous contact force models for impact analysis in multibody systems. *Nonlinear Dynamics 5*, 2 (1994), 193-207.

[16] MCGEER, T. Passive dynamic walking. *International Journal of Robotics Research 9*, 2 (1990), 62-82.

[17] MODARRES NAJAFABADI, S.A., KÖVECSES, J., AND ANGELES, J. A comparative study of approaches to dynamics modeling of contact transitions in multibody systems. In *Proc. ASME Int. Design Eng. Tech. Conferences IDETC'05*, Long Beach, CA, USA, 2005.

[18] NOREAU, L., RICHARDS, C. L., COMEAU, F., AND TARDIF, D. Biomechanical analysis of swing-through gait in paraplegic and non-disabled individuals. *J. of Biomechanics 28*, 6 (1995), 689-700.

[19] STRONGE, W. J. *Impact Mechanics*. Cambridge: Cambridge University Press, 2000.

[20] WINTER, D. A. *Biomechanics and Motor Control of Human Movement*. Hoboken: John Wiley & Sons, 2005.